A&A 590, L6 (2016)
DOI: 10.1051/0004-6361/201628612

Astronomy & Astrophysics

Letter to the Editor

The ALMA-PILS survey: First detections of deuterated formamide and deuterated isocyanic acid in the interstellar medium

A. Coutens[1], J. K. Jørgensen[2], M. H. D. van der Wiel[2], H. S. P. Müller[3], J. M. Lykke[2], P. Bjerkeli[2,4], T. L. Bourke[5], H. Calcutt[2], M. N. Drozdovskaya[6], C. Favre[7], E. C. Fayolle[8], R. T. Garrod[9], S. K. Jacobsen[2], N. F. W. Ligterink[6], K. I. Öberg[8], M. V. Persson[6], E. F. van Dishoeck[6,10], and S. F. Wampfler[2]

[1] Department of Physics and Astronomy, University College London, Gower St., London, WC1E 6BT, UK
e-mail: a.coutens@ucl.ac.uk
[2] Centre for Star and Planet Formation, Niels Bohr Institute & Natural History Museum of Denmark, University of Copenhagen, Øster Voldgade 5-7, 1350 Copenhagen K., Denmark
[3] I. Physikalisches Institut, Universität zu Köln, Zülpicher Str. 77, 50937 Köln, Germany
[4] Department of Earth and Space Sciences, Chalmers University of Technology, Onsala Space Observatory, 439 92 Onsala, Sweden
[5] SKA Organization, Jodrell Bank Observatory, Lower Withington, Macclesfield, Cheshire SK11 9DL, UK
[6] Leiden Observatory, Leiden University, PO Box 9513, 2300 RA Leiden, The Netherlands
[7] Institut de Planétologie et d'Astrophysique de Grenoble, UMR 5274, UJF-Grenoble 1/CNRS, 38041 Grenoble, France
[8] Harvard-Smithsonian Center for Astrophysics, 60 Garden Street, Cambridge, MA 02138, USA
[9] Departments of Chemistry and Astronomy, University of Virginia, Charlottesville, VA 22904, USA
[10] Max-Planck Institut für Extraterrestrische Physik (MPE), Giessenbachstr. 1, 85748 Garching, Germany

Received 31 March 2016 / Accepted 6 May 2016

ABSTRACT

Formamide (NH_2CHO) has previously been detected in several star-forming regions and is thought to be a precursor for different prebiotic molecules. Its formation mechanism is still debated, however. Observations of formamide, related species, and their isopotologues may provide useful clues to the chemical pathways leading to their formation. The Protostellar Interferometric Line Survey (PILS) represents an unbiased, high angular resolution and sensitivity spectral survey of the low-mass protostellar binary IRAS 16293–2422 with the Atacama Large Millimeter/submillimeter Array (ALMA). For the first time, we detect the three singly deuterated forms of NH_2CHO (NH_2CDO, cis- and trans-NHDCHO), as well as DNCO towards the component B of this binary source. The images reveal that the different isotopologues are all present in the same region. Based on observations of the ^{13}C isotopologues of formamide and a standard $^{12}C/^{13}C$ ratio, the deuterium fractionation is found to be similar for the three different forms with a value of about 2%. The DNCO/HNCO ratio is also comparable to the D/H ratio of formamide (~1%). These results are in agreement with the hypothesis that NH_2CHO and HNCO are chemically related through grain-surface formation.

Key words. astrochemistry – stars: formation – stars: protostars – ISM: molecules – ISM: individual objects: IRAS 16293-2422 – astrobiology

1. Introduction

Formamide (NH_2CHO), also known as methanamide, contains the amide bond (–N–C(=O)–), which plays an important role in the synthesis of proteins. This molecule is a precursor for potential compounds of genetic and metabolic interest (Saladino et al. 2012). Interestingly, it is present in various astrophysical environments: high-mass star-forming regions (e.g. Bisschop et al. 2007; Adande et al. 2013), low-mass protostars (Kahane et al. 2013; López-Sepulcre et al. 2015), shocked regions (Yamaguchi et al. 2012; Mendoza et al. 2014), a translucent cloud (Corby et al. 2015), comets (Bockelée-Morvan et al. 2000; Biver et al. 2014; Goesmann et al. 2015), and even an extragalactic source (Muller et al. 2013).

The formation of formamide is still not clearly understood: several routes have been proposed, both in the gas phase and on the grain surfaces. In the gas phase, many ion-molecule reactions have been ruled out as not sufficiently efficient owing to endothermicity or high-energy barriers (see e.g. Redondo et al. 2014a,b). A neutral-neutral reaction between H_2CO and NH_2 was, however, shown to be barrierless and could account for the abundance of formamide in some sources (Barone et al. 2015). On the grain surface, it has been suggested that formamide forms through the reaction between HCO and NH_2 (Jones et al. 2011; Garrod 2013) and/or hydrogenation of isocyanic acid, HNCO. In particular, the latter suggestion is supported by a strong correlation between the HNCO and NH_2CHO abundances in different sources (Bisschop et al. 2007; Mendoza et al. 2014; López-Sepulcre et al. 2015). However, an experiment based on the H-bombardment of HNCO at low temperature has recently shown that this reaction is not efficient in cold environments (Noble et al. 2015). Instead, other pathways to HNCO and NH_2CHO on grains have been suggested, either with or without UV or ion bombardment (see e.g. Kaňuchová et al. 2016, and references therein).

Measurements of isotopic fractionation may help to constrain formation pathways of molecules since isotopic fractionation (especially deuteration) is sensitive to physical conditions such as density and temperature. Until recently, the study of deuteration in solar-type protostars was mainly limited

to relatively small and abundant molecules, such as H_2O, HCO^+, HCN, H_2CO, and CH_3OH. Even though the deuterium fractionation is known to be enhanced in low-mass protostars (see e.g. Ceccarelli et al. 2007), measurements of lines of deuterated complex organic molecules (COMs) still require high-sensitivity observations. So far, only deuterated methyl formate and dimethyl ether have been detected towards the low-mass protostar IRAS 16293–2422 (hereafter IRAS 16293) by Demyk et al. (2010) and Richard et al. (2013). With the Atacama Large Millimeter/submillimeter Array (ALMA), it is now possible to search for the isotopologues of complex and less abundant species. In this Letter, we report the first detection of the three singly deuterated forms of formamide, as well as DNCO towards IRAS 16293. These observations mark the first detections of those isotopologues in the interstellar medium.

2. Observations

An ALMA unbiased spectral survey of the binary protostar IRAS16293 was recently carried out in the framework of the Protostellar Interferometric Line Survey[1] (PILS; Jørgensen et al. 2016). The observations were centered on a position at equal distance between the sources A and B that are separated by ~5″. A full description of the survey and the data reduction can be found in Jørgensen et al. (2016). For this work, we use the part of the large spectral survey obtained in Band 7 between 329.15 GHz and 362.90 GHz, both with the 12 m array and the Atacama Compact Array (ACA). The spectral resolution of these observations is 0.244 MHz (i.e. ~0.2 km s^{-1}). After combining the 12 m and ACA data, the final spectral line datacubes show a sensitivity that is better than 5 mJy beam^{-1} km s^{-1}. The beam sizes range between 0.4″ and 0.7″. Additional observations in Bands 3 and 6 cover narrow spectral ranges and, consequently, a very limited number of transitions of formamide isotopologues. After the analysis of Band 7, we checked that the results are consistent with these lower frequency observations.

3. Analysis and results

To search for the isotopologues of formamide, we use the spectrum extracted at the same position as in Lykke et al. (in prep.), i.e. a position offset by ~0.5″ from the continuum peak of source B in the south west direction (α_{J2000} = 16^{h}32^{m}22^s.58, δ_{J2000} = −24°28′32.8″). Although the lines are brighter at the position of the continuum peak, the presence of both absorption and emission makes analysis difficult. At the selected position, most of the lines present Gaussian profiles and are relatively bright compared to other positions. In source A, the lines are quite broad, leading to significant line confusion that prevents the search for isotopologues of complex species (e.g. Jørgensen et al. 2012). This Letter is therefore focused on source B only.

Using the CASSIS[2] software, we identify several unblended lines that can be assigned to the three singly deuterated forms of NH_2CHO and to $NH_2{}^{13}CHO$, DNCO, and $HN^{13}CO$ (see Table 1). These mark the first detections of NH_2CDO, cis-NHDCHO, trans-NHDCHO, and DNCO in the interstellar medium. The list of unblended lines can be found in the Appendix. Maps of the integrated line emission from representative lines from the different isotopologues towards source B are shown in Fig. 1. The emission of the different lines clearly arise from a similar compact region in the vicinity of IRAS16293B.

[1] http://youngstars.nbi.dk/PILS/
[2] http://cassis.irap.omp.eu/

Table 1. Number of lines used in the analysis of the isotopologues of NH_2CHO and HNCO and column densities derived for T_{ex} = 300 K and a source size of 0.5″.

Species	# of lines	E_{up} (K)	N (cm^{-2})
NH_2CDO	12	146–366	2.1×10^{14}
cis-NHDCHO	11	146–307	2.1×10^{14}
trans-NHDCHO	11	151–332	1.8×10^{14}
$NH_2{}^{13}CHO$	10	152–428	1.5×10^{14}
$^{15}NH_2CHO$	–	–	$\leq1.0\times10^{14a}$
$NH_2CH^{18}O$	–	–	$\leq0.8\times10^{14a}$
DNCO	4	150–751	3.0×10^{14}
$HN^{13}CO$	8	127–532	4.0×10^{14}
$H^{15}NCO$	–	–	$\leq2.0\times10^{14a}$
$HNC^{18}O$	–	–	$\leq1.5\times10^{14a}$

Notes. [(a)] 3σ upper limit.

A hole is observed in the maps owing to the absorptions that are produced against the strong continuum at the continuum peak position. For DNCO, the larger beam size for the observations of this transition masks the absorption. The spatial variations that are observed among the different species are probably due to different line excitation or line brightness. In particular, HNCO seems to be slightly more extended than NH_2CHO, but this is most likely due to the fact that the HNCO lines are particularly bright compared to the HNCO and formamide isotopologues.

To constrain the excitation temperatures and column densities of the different species, we produce a grid of synthetic spectra, assuming local thermodynamical equilibrium (LTE). We predict the spectra for different excitation temperatures between 100 and 300 K with a step of 25 K and for different column densities between 1×10^{13} and 1×10^{17} cm^{-2}. First, the column density is roughly estimated using relatively large steps, then refined using smaller steps around the best-fit solution. We determine the best-fit model using a χ^2 method, comparing the observed and synthetic spectra at ±0.5 MHz around the rest frequency of the predicted emission lines. We carefully check that the best-fit model does not predict any lines that are not observed in the spectra. For the deuterated forms, the models are in agreement with the observations for excitation temperatures between 100 and 300 K. However, for $NH_2{}^{13}CHO$ and $HN^{13}CO$, a model with a high excitation temperature better reproduces the observed emission than a model with a low excitation temperature (see Figs. B.4 and B.6). An excitation temperature of 300 K was consequently adopted for the analysis of the different isotopologues. This excitation temperature is similar to that derived for glycolaldehyde and ethylene glycol (Jørgensen et al. 2012, 2016), but higher than what is found for acetaldehyde, ethylene oxide, and propanal (~125 K, Lykke et al., in prep.). The derived column densities, assuming a linewidth of 1 km s^{-1} and a source size of 0.5″ (Jørgensen et al. 2016; Lykke et al., in prep.), are summarized in Table 1. The uncertainties on the column densities are all estimated to be within a factor of 2 (including the uncertainty on both the excitation temperature and the baseline subtraction). The upper limits are estimated visually by a comparison of the synthetic spectra with the observations on the entire spectral range. Figure 2 shows three lines of each isotopologue with the best-fit model. The models for all the lines are shown in Appendix B.

The column densities of $NH_2{}^{13}CHO$, and $HN^{13}CO$ are estimated to be 1.5×10^{14} cm^{-2} and 4×10^{14} cm^{-2}, respectively. Assuming a $^{12}C/^{13}C$ ratio of 68 (Milam et al. 2005), the column densities for the main isotopologues of formamide and isocyanic acid are predicted to be 1×10^{16} cm^{-2} and 3×10^{16} cm^{-2}. With

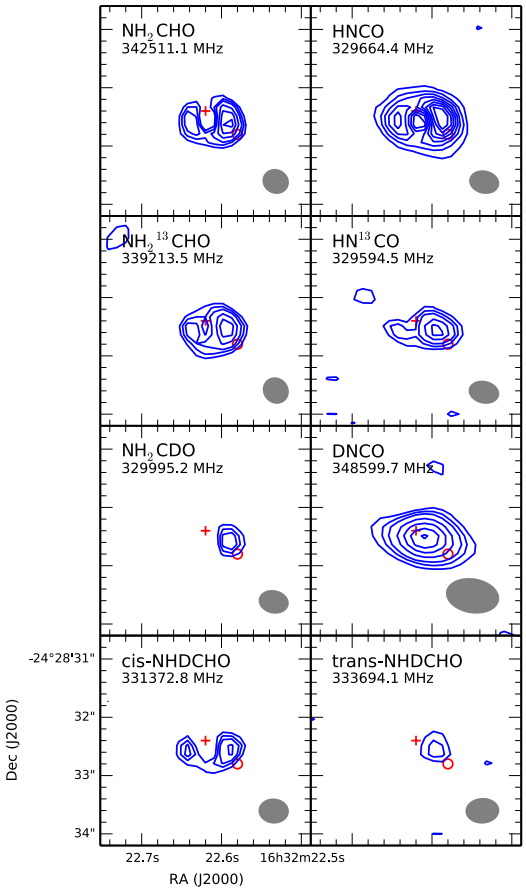

Fig. 1. Integrated intensity maps of NH_2CHO, HNCO, and their isotopologues towards source B. The position of the continuum peak of source B is indicated with a red cross, while the position of where the spectrum was extracted is shown with a red circle. The beam sizes are shown in gray in the bottom right corner of each panel. The contour levels start for the main isotopologue of HNCO at 0.05 Jy km s^{-1} with a step of 0.05 Jy km s^{-1}. For the other species, the levels are 0.02, 0.03, 0.04, 0.06, 0.08, 0.1, and 0.12 Jy km s^{-1}.

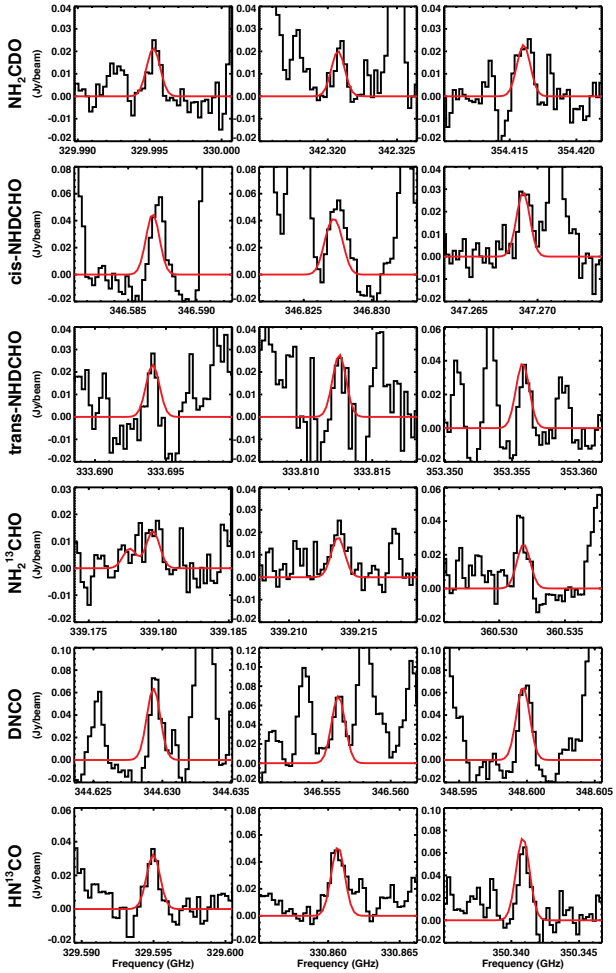

Fig. 2. Black: detected lines of NH_2CDO, cis-NHDCHO, trans-NHDCHO, $NH_2^{13}CHO$, DNCO, and $HN^{13}CO$. Red: best-fit model.

these column densities, several NH_2CHO lines and all of the HNCO lines are overproduced, indicating that they are optically thick. The model of formamide is, however, in agreement with the few lines with the lowest opacities (see Figs. B.7 and B.8). $NH_2CH^{18}O$ has also been searched for, but is not detected with a 3σ upper limit of 8×10^{13} cm^{-2}. The non-detection of this isotopologue is consistent with the $^{16}O/^{18}O$ ratio of 560 in the interstellar medium (Wilson 1999), which gives $N(NH_2CH^{18}O) = 2\times10^{13}$ cm^{-2}. Similarly, $HNC^{18}O$ is not detected either with a 3σ upper limit of 1.5×10^{14} cm^{-2}, which is consistent with its expected column density of 5×10^{13} cm^{-2}.

Using the column densities derived for the ^{13}C isotopologues and a standard $^{12}C/^{13}C$ ratio, the deuterium fractionation in NH_2CHO is about 2% for the three deuterated forms and the DNCO/HNCO ratio is similar (~1%). If the $^{12}C/^{13}C$ ratio is lower (~30) as reported for glycolaldehyde by Jørgensen et al. (2016), the D/H ratios of formamide and isocyanic acid would be about 4–5% and 2–3%, respectively.

We also search for the ^{15}N isotopologues of formamide and isocyanic acid. A couple of transitions could tentatively be assigned to $^{15}NH_2CHO$, but these lines are close to the noise level and possibly blended with other species. For $H^{15}NCO$, the uncertainties on the frequencies of some of the transitions are rather large, preventing any firm detection. Based on a standard $^{12}C/^{13}C$ ratio, lower limits of 100 and 138 are obtained for the $^{14}N/^{15}N$ ratios of formamide and HNCO respectively.

4. Discussion and conclusion

Our derived ratio in IRAS16293 for $HNCO/NH_2CHO$, ~3, is consistent with the ratios found in warm sources in previous studies (Bisschop et al. 2007; Mendoza et al. 2014; López-Sepulcre et al. 2015). Thanks to our interferometric observations, we also confirm that these two species are spatially correlated. The deuterium fractionation ratios of these two molecules are also similar, reinforcing the hypothesis that they are chemically related. We discuss here possible scenarios for the formation of these species in the warm inner regions of protostars.

Assuming that the deuteration of formaldehyde in the region probed by the ALMA observations of formamide is similar to the value derived with single-dish observations (~15%, Loinard et al. 2000), we can discuss the possibility for the gas-phase formation mechanism proposed by Barone et al. (2015), $H_2CO + NH_2 \rightarrow NH_2CHO + H$. According to this reaction, the deuterated form NHDCHO would result from the reaction between NHD and H_2CO, while NH_2CDO would form from NH_2 and HDCO. We would consequently expect a higher deuteration for NH_2CDO, compared to the observations, unless the reaction between NH_2 and HDCO leads more efficiently to NH_2CHO

and D, compared to NH_2CDO and H. Theoretical or experimental studies of the branching ratios of these reactions would be needed to rule out this scenario. The determination of the $HDCO/H_2CO$ ratio from the PILS survey is also necessary. Nevertheless, it should be noted that, so far, there is no proposed scenario in the gas phase that could explain the correlation with HNCO.

Although it was recently shown that NH_2CHO does not form by hydrogenation of HNCO on grain surfaces (Noble et al. 2015), several other proposed mechanisms exist in the literature. Both species can be formed through barrierless reactions in ices through NH + CO → HNCO and NH_2 + H_2CO → NH_2CHO + H, as demonstrated experimentally (Fedoseev et al. 2015, 2016). Alternatively, both species are formed through ion bombardment of H_2O:CH_4:N_2 mixtures (Kaňuchová et al. 2016) or UV irradiation of CO:NH_3:CH_3OH and/or HNCO mixtures (e.g. Demyk et al. 1998; Raunier et al. 2004; Jones et al. 2011; Henderson & Gudipati 2015). Quantitative gas-grain modeling under conditions representative of IRAS16293 are needed to assess which of these grain surface routes dominates.

Ultimately, the HNCO and NH_2CHO deuterium fractionation level and pattern may also hold a clue to their formation routes. A particularly interesting result is that the three singly deuterated forms of formamide are found with similar abundances in IRAS16293. Contrary to the -CH functional group that is not affected by hydrogen isotope exchanges, the hydroxyl (-OH) and amine (-NH) groups are expected to establish hydrogen bonds and equilibrate with water (Faure et al. 2015). This mechanism was proposed to explain the different CH_3OD/CH_3OH (~1.8%) and CH_2DOH/CH_3OH (~37%) ratios derived in IRAS16293 (Parise et al. 2006), as the water deuterium fractionation of water in the upper layers of the grain mantles, where complex organic molecules form, is about a few percent (Coutens et al. 2012, 2013; Furuya et al. 2016). We do not see these types of differences for formamide, for which all forms show a deuterium fractionation similar to the CH_3OD/CH_3OH ratio and water. The deuterium fractionation of methanol from the PILS data needs to be investigated to know if the different deuterium fractionation ratios of the -CH and -OH groups are also observed at small scales.

In conclusion, in this Letter we present the first detection of the three singly deuterated forms of formamide and DNCO. The similar deuteration of these species and their similar spatial distributions favors the formation of these two species on grain surfaces. Further studies are, however, needed to rule out gas phase routes. These detections illustrate the strength of ALMA, and large spectral surveys such as PILS in particular, for the detections of deuterated complex molecules. Determinations of the deuterium fractionation for more complex molecules will help to constrain their formation pathways. The search for deuterated formamide in more sources is needed to reveal how variable the deuteration of formamide is, and if the similarity of the abundances of the three deuterated forms is common.

Acknowledgements. The authors thank Gleb Fedoseev and Harold Linnartz for fruitful discussions. This paper makes use of the following ALMA data: ADS/JAO.ALMA#2013.1.00278.S. ALMA is a partnership of ESO (representing its member states), NSF (USA) and NINS (Japan), together with NRC (Canada) and NSC and ASIAA (Taiwan), in cooperation with the Republic of Chile. The Joint ALMA Observatory is operated by ESO, AUI/NRAO and NAOJ. The work of A.C. was funded by an STFC grant. A.C. thanks the COST action CM1401 Our Astrochemical History for additional financial support. The group of J.K.J. acknowledges support from a Lundbeck Foundation Group Leader Fellowship, as well as the European Research Council (ERC) under the European Union's Horizon 2020 research and innovation programme (grant agreement No 646908) through ERC Consolidator Grant S4F. Research at the Centre for Star and Planet Formation is funded by the Danish National Research Foundation. The group of E.v.D. acknowledges A-ERC grant 291141 CHEMPLAN.

References

Adande, G. R., Woolf, N. J., & Ziurys, L. M. 2013, Astrobiol., 13, 439
Barone, V., Latouche, C., Skouteris, D., et al. 2015, MNRAS, 453, L31
Bisschop, S. E., Jørgensen, J. K., van Dishoeck, E. F., & de Wachter, E. B. M. 2007, A&A, 465, 913
Biver, N., Bockelée-Morvan, D., Debout, V., et al. 2014, A&A, 566, L5
Blanco, S., Lopez, J. C., Lessari, A., & Alonso, J. L. 2006, J. Am. Chem. Soc., 128, 12111
Bockelée-Morvan, D., Lis, D. C., Wink, J. E., et al. 2000, A&A, 353, 1101
Ceccarelli, C., Caselli, P., Herbst, E., Tielens, A. G. G. M., & Caux, E. 2007, Protostars and Planets V, 47
Corby, J. F., Jones, P. A., Cunningham, M. R., et al. 2015, MNRAS, 452, 3969
Coutens, A., Vastel, C., Caux, E., et al. 2012, A&A, 539, A132
Coutens, A., Vastel, C., Cazaux, S., et al. 2013, A&A, 553, A75
Demyk, K., Dartois, E., D'Hendecourt, L., et al. 1998, A&A, 339, 553
Demyk, K., Bottinelli, S., Caux, E., et al. 2010, A&A, 517, A17
Faure, A., Faure, M., Theulé, P., Quirico, E., & Schmitt, B. 2015, A&A, 584, A98
Fedoseev, G., Ioppolo, S., Zhao, D., Lamberts, T., & Linnartz, H. 2015, MNRAS, 446, 439
Fedoseev, G., Chuang, K.-J., van Dishoeck, E. F., Ioppolo, S., & Linnartz, H. 2016, MNRAS, in press
Furuya, K., van Dishoeck, E. F., & Aikawa, Y. 2016, A&A, 586, A127
Gardner, F. F., Godfrey, P. D., & Williams, D. R. 1980, MNRAS, 193, 713
Garrod, R. T. 2013, ApJ, 765, 60
Goesmann, F., Rosenbauer, H., Bredehöft, J. H., et al. 2015, Science, 349, 020689
Henderson, B. L., & Gudipati, M. S. 2015, ApJ, 800, 66
Hirota, E., Sugisaki, R., Nielsen, C. J., & Sørensen, G. O. 1974, J. Mol. Spectr., 49, 251
Hocking, W. H., Gerry, M. C. L., & Winnewisser, G. 1975, Can. J. Phys., 53, 1869
Jones, B. M., Bennett, C. J., & Kaiser, R. I. 2011, ApJ, 734, 78
Jørgensen, J. K., Favre, C., Bisschop, S. E., et al. 2012, ApJ, 757, L4
Jørgensen, J. K., van der Wiel, M. H. D., Coutens, A., et al. 2016, A&A, submitted
Kahane, C., Ceccarelli, C., Faure, A., & Caux, E. 2013, ApJ, 763, L38
Kaňuchová, Z., Urso, R. G., Baratta, G. A., et al. 2016, A&A, 585, A155
Kryvda, A. V., Gerasimov, V. G., Dyubko, S. F., Alekseev, E. A., & Motiyenko, R. A. 2009, J. Mol. Spectr., 254, 28
Kukolich, S. G., & Nelson, A. C. 1971, Chem. Phys. Lett., 11, 383
Kurland, R. J., & Bright Wilson, Jr., E. 1957, J. Chem. Phys., 27, 585
Kutsenko, A. S., Motiyenko, R. A., Margulès, L., & Guillemin, J.-C. 2013, A&A, 549, A128
Lapinov, A. V., Golubiatnikov, G. Y., Markov, V. N., & Guarnieri, A. 2007, Astron. Lett., 33, 121
Loinard, L., Castets, A., Ceccarelli, C., et al. 2000, A&A, 359, 1169
López-Sepulcre, A., Jaber, A. A., Mendoza, E., et al. 2015, MNRAS, 449, 2438
Mendoza, E., Lefloch, B., López-Sepulcre, A., et al. 2014, MNRAS, 445, 151
Milam, S. N., Savage, C., Brewster, M. A., Ziurys, L. M., & Wyckoff, S. 2005, ApJ, 634, 1126
Moskienko, E. M., & Dyubko, S. F. 1991, Radiophys. Quant. Electron., 34, 181
Motiyenko, R. A., Tercero, B., Cernicharo, J., & Margulès, L. 2012, A&A, 548, A71
Müller, H. S. P., Thorwirth, S., Roth, D. A., & Winnewisser, G. 2001, A&A, 370, L49
Müller, H. S. P., Schlöder, F., Stutzki, J., & Winnewisser, G. 2005, J. Mol. Struct., 742, 215
Muller, S., Beelen, A., Black, J. H., et al. 2013, A&A, 551, A109
Niedenhoff, M., Yamada, K. M. T., Belov, S. P., & Winnewisser, G. 1995, J. Mol. Spectr., 174, 151
Noble, J. A., Theule, P., Congiu, E., et al. 2015, A&A, 576, A91
Parise, B., Ceccarelli, C., Tielens, A. G. G. M., et al. 2006, A&A, 453, 949
Pickett, H. M., Poynter, R. L., Cohen, E. A., et al. 1998, J. Quant. Spectr. Rad. Transf., 60, 883
Raunier, S., Chiavassa, T., Duvernay, F., et al. 2004, A&A, 416, 165
Redondo, P., Barrientos, C., & Largo, A. 2014a, ApJ, 793, 32
Redondo, P., Barrientos, C., & Largo, A. 2014b, ApJ, 780, 181
Richard, C., Margulès, L., Caux, E., et al. 2013, A&A, 552, A117
Saladino, R., Crestini, C., Pino, S., Costanzo, G., & Di Mauro, E. 2012, Physics of Life Reviews, 9, 84
Vorob'eva, E. M., & Dyubko, S. F. 1994, Radiophys. Quant. Electron., 37, 155
Wilson, T. L. 1999, Rep. Progr. Phys., 62, 143
Yamaguchi, T., Takano, S., Watanabe, Y., et al. 2012, PASJ, 64, 105

Appendix A: Spectroscopic data

A list of unblended and optically thin lines used in the analysis is presented in Table A.1. The spectroscopic data for NH_2CHO $v = 0$, NH_2CHO $v_{12} = 1$, $NH_2{}^{13}CHO$, $^{15}NH_2CHO$, $NH_2CH^{18}O$, NH_2CDO, cis-NHDCHO, trans-NHDCHO (Kurland & Bright Wilson 1957; Kukolich & Nelson 1971; Hirota et al. 1974; Gardner et al. 1980; Moskienko & Dyubko 1991; Vorob'eva & Dyubko 1994; Blanco et al. 2006; Kryvda et al. 2009; Motiyenko et al. 2012; Kutsenko et al. 2013) and HNCO (Kukolich & Nelson 1971; Hocking et al. 1975; Niedenhoff et al. 1995; Lapinov et al. 2007) come from the Cologne Database for Molecular Spectroscopy (CMDS, Müller et al. 2001, 2005), while the data for DNCO, $HN^{13}CO$, $H^{15}NCO$ and $HNC^{18}O$ (Hocking et al. 1975) are taken from the Jet Propulsion Laboratory (JPL) database (Pickett et al. 1998). It should be noted that there are significant differences for the predicted frequencies of the main isotopologue of NH_2CHO between CDMS and JPL (>1 MHz). A better agreement is found with the observations for the most recent entry in CDMS. For some of the HNCO isotopologues, there is a lack of published spectroscopic data at high frequencies. In particular for $H^{15}NCO$, the range of uncertainty for some of the frequencies is quite high. As the $HN^{13}CO$ transitions all appeared slightly shifted, compared to the observations, we applied a correction of +0.5 MHz to model the lines.

The column densities of the formamide isotopologues given in Table 1 were corrected by a factor of 1.5 to take into account the contribution of the vibrational states for an excitation temperature of 300 K.

Table A.1. Detected lines of NH_2CHO, HNCO and their isotopologues used in the analysis.

Species	Transition	Frequency (MHz)	E_{up} (K)	A_{ij} (s^{-1})	g_{up}
NH_2CDO	(17 0 17–16 0 16)	329 995.2	145.6	2.64×10^{-3}	105
NH_2CDO	(16 9 7–15 9 6)	333 363.6	308.9	1.87×10^{-3}	99
NH_2CDO	(16 9 8–15 9 7)	333 363.6	308.9	1.87×10^{-3}	99
NH_2CDO	(16 7 10–15 7 9)	333 696.6	240.7	2.22×10^{-3}	99
NH_2CDO	(16 7 9–15 7 8)	333 696.6	240.7	2.22×10^{-3}	99
NH_2CDO	(16 4 13–15 4 12)	335 234.9	170.5	2.61×10^{-3}	99
NH_2CDO	(16 3 13–15 3 12)	342 320.7	156.9	2.86×10^{-3}	99
NH_2CDO	(17 1 16–16 1 15)	351 988.3	158.1	3.18×10^{-3}	105
NH_2CDO	(17 10 7–16 10 6)	354 151.5	366.4	2.15×10^{-3}	105
NH_2CDO	(17 10 8–16 10 7)	354 151.5	366.4	2.15×10^{-3}	105
NH_2CDO	(17 9 8–16 9 7)	354 257.0	325.9	2.37×10^{-3}	105
NH_2CDO	(17 9 9–16 9 8)	354 257.0	325.9	2.37×10^{-3}	105
NH_2CDO	(17 8 10–16 8 9)	354 416.0	289.6	2.56×10^{-3}	105
NH_2CDO	(17 8 9–16 8 8)	354 416.0	289.6	2.56×10^{-3}	105
NH_2CDO	(17 7 11–16 7 10)	354 661.3	257.7	2.74×10^{-3}	105
NH_2CDO	(17 7 10–16 7 9)	354 661.3	257.7	2.74×10^{-3}	105
NH_2CDO	(17 5 12–16 5 11)	355 800.2	206.7	3.04×10^{-3}	105
NH_2CDO	(17 4 13–16 4 12)	357 938.5	187.8	3.20×10^{-3}	105
cis-NHDCHO	(16 3 13–15 3 12)	331 372.8	156.0	2.59×10^{-3}	99
cis-NHDCHO	(16 2 14–15 2 13)	337 248.5	146.0	2.79×10^{-3}	99
cis-NHDCHO	(17 2 16–16 2 15)	340 520.3	158.0	2.87×10^{-3}	105
cis-NHDCHO	(18 1 18–17 1 17)	344 878.9	160.8	3.02×10^{-3}	111
cis-NHDCHO	(17 8 10–16 8 9)	346 444.0	306.6	2.39×10^{-3}	105
cis-NHDCHO	(17 8 9–16 8 8)	346 444.0	306.6	2.39×10^{-3}	105
cis-NHDCHO	(17 7 11–16 7 10)	346 586.8	269.8	2.56×10^{-3}	105
cis-NHDCHO	(17 7 10–16 7 9)	346 586.8	269.8	2.56×10^{-3}	105
cis-NHDCHO	(17 6 12–16 6 11)	346 826.8	238.0	2.70×10^{-3}	105
cis-NHDCHO	(17 6 11–16 6 10)	346 827.5	238.0	2.70×10^{-3}	105
cis-NHDCHO	(17 3 15–16 3 14)	347 115.8	172.0	2.99×10^{-3}	105
cis-NHDCHO	(17 5 12–16 5 11)	347 268.9	211.1	2.83×10^{-3}	105
cis-NHDCHO	(17 4 14–16 4 13)	347 827.8	189.2	2.94×10^{-3}	105
cis-NHDCHO	(17 3 14–16 3 13)	353 047.5	173.0	3.15×10^{-3}	105
trans-NHDCHO	(17 8 9–16 8 8)	333 628.6	332.4	2.14×10^{-3}	105
trans-NHDCHO	(17 8 10–16 8 9)	333 628.6	332.4	2.14×10^{-3}	105
trans-NHDCHO	(17 7 11–16 7 10)	333 694.1	288.3	2.28×10^{-3}	105
trans-NHDCHO	(17 7 10–16 7 9)	333 694.1	288.3	2.28×10^{-3}	105
trans-NHDCHO	(17 6 12–16 6 11)	333 812.6	250.1	2.41×10^{-3}	105
trans-NHDCHO	(17 6 11–16 6 10)	333 812.7	250.1	2.41×10^{-3}	105
trans-NHDCHO	(17 4 14–16 4 13)	334 403.2	191.4	2.61×10^{-3}	105
trans-NHDCHO	(18 1 18–17 1 17)	336 945.3	157.3	2.82×10^{-3}	111
trans-NHDCHO	(18 0 18–17 0 17)	338 818.4	156.9	2.87×10^{-3}	111
trans-NHDCHO	(17 1 16–16 1 15)	338 878.8	150.6	2.86×10^{-3}	105
trans-NHDCHO	(18 7 12–17 7 11)	353 355.8	305.2	2.77×10^{-3}	111
trans-NHDCHO	(18 7 11–17 7 10)	353 355.8	305.2	2.77×10^{-3}	111
trans-NHDCHO	(18 5 14–17 5 13)	353 758.4	234.7	3.02×10^{-3}	111
trans-NHDCHO	(18 3 16–17 3 15)	354 028.8	187.8	3.19×10^{-3}	111
trans-NHDCHO	(18 4 15–17 4 14)	354 185.9	208.4	3.13×10^{-3}	111
$NH_2{}^{13}CHO$	(16 10 6–15 10 5)	339 170.1	427.9	1.75×10^{-3}	33
$NH_2{}^{13}CHO$	(16 10 7–15 10 6)	339 170.1	427.9	1.75×10^{-3}	33
$NH_2{}^{13}CHO$	(16 9 7–15 9 6)	339 179.6	373.0	1.97×10^{-3}	33
$NH_2{}^{13}CHO$	(16 9 8–15 9 7)	339 179.6	373.0	1.97×10^{-3}	33
$NH_2{}^{13}CHO$	(16 8 8–15 8 7)	339 213.5	323.8	2.16×10^{-3}	33
$NH_2{}^{13}CHO$	(16 8 9–15 8 8)	339 213.5	323.8	2.16×10^{-3}	33
$NH_2{}^{13}CHO$	(16 5 11–15 5 10)	339 672.1	210.9	2.61×10^{-3}	33
$NH_2{}^{13}CHO$	(16 4 13–15 4 12)	340 090.4	184.9	2.72×10^{-3}	33
$NH_2{}^{13}CHO$	(16 4 12–15 4 11)	340 273.4	184.9	2.73×10^{-3}	33
$NH_2{}^{13}CHO$	(17 1 17–16 1 16)	342 156.0	151.5	2.95×10^{-3}	35
$NH_2{}^{13}CHO$	(17 9 8–16 9 7)	360 396.3	390.3	2.49×10^{-3}	35
$NH_2{}^{13}CHO$	(17 9 9–16 9 8)	360 396.3	390.3	2.49×10^{-3}	35
$NH_2{}^{13}CHO$	(17 7 11–16 7 10)	360 531.8	297.7	2.88×10^{-3}	35

Notes. This list only includes optically thin and unblended lines.

Table A.1. continued.

Species	Transition	Frequency (MHz)	E_{up} (K)	A_{ij} (s^{-1})	g_{up}
$NH_2{}^{13}CHO$	(17 7 10–16 7 9)	360 531.8	297.7	2.88×10^{-3}	35
$NH_2{}^{13}CHO$	(18 1 18–17 1 17)	361 904.8	168.9	3.49×10^{-3}	37
NH_2CHO $v=0$	(16 3 14–16 2 15)	331 685.9	165.6	7.87×10^{-5}	33
NH_2CHO $v=0$	(8 2 7–7 1 6)	334 483.5	48.5	5.49×10^{-5}	17
NH_2CHO $v=0$	(17 3 15–17 2 16)	336 733.0	183.0	8.2×10^{-5}	35
NH_2CHO $v=0$	(34 3 31–34 2 32)	342 029.5	645.9	1.07×10^{-4}	69
NH_2CHO $v=0$	(18 3 16–18 2 17)	342 511.1	201.3	8.57×10^{-5}	37
NH_2CHO $v=0$	(28 4 24–28 3 25)	344 545.8	464.1	1.15×10^{-4}	57
NH_2CHO $v=0$	(19 3 17–19 2 18)	349 051.7	220.7	8.99×10^{-5}	39
NH_2CHO $v=0$	(20 3 18–20 2 19)	356 379.8	241.1	9.47×10^{-5}	41
NH_2CHO $v=0$	(20 1 19–19 2 18)	359 119.4	221.2	8.45×10^{-5}	41
NH_2CHO $v_{12}=1$	(17 14 3–16 14 2)	360 717.7	1144.3	1.12×10^{-3}	35
NH_2CHO $v_{12}=1$	(17 14 4–16 14 3)	360 717.7	1144.3	1.12×10^{-3}	35
DNCO	(17 1 17 18–16 1 16 17)	344 629.4	172.9	5.92×10^{-4}	37
DNCO	(17 1 17 17–16 1 16 16)	344 629.4	172.9	5.90×10^{-4}	35
DNCO	(17 1 17 16–16 1 16 15)	344 629.4	172.9	5.90×10^{-4}	33
DNCO	(17 0 17 18–16 0 16 17)	346 556.2	149.7	6.04×10^{-4}	37
DNCO	(17 0 17 17–16 0 16 16)	346 556.2	149.7	6.02×10^{-4}	35
DNCO	(17 0 17 16–16 0 16 15)	346 556.2	149.7	6.02×10^{-4}	33
DNCO	(17 5 12 18–16 5 11 17)	346 714.9	750.6	5.53×10^{-4}	37
DNCO	(17 5 13 18–16 5 12 17)	346 714.9	750.6	5.53×10^{-4}	37
DNCO	(17 5 13 16–16 5 12 15)	346 714.9	750.6	5.50×10^{-4}	33
DNCO	(17 5 12 16–16 5 11 15)	346 714.9	750.6	5.50×10^{-4}	33
DNCO	(17 5 13 17–16 5 12 16)	346 714.9	750.6	5.51×10^{-4}	35
DNCO	(17 5 12 17–16 5 11 16)	346 714.9	750.6	5.51×10^{-4}	35
DNCO	(17 1 16 18–16 1 15 17)	348 599.7	174.6	6.13×10^{-4}	37
DNCO	(17 1 16 17–16 1 15 16)	348 599.7	174.6	6.10×10^{-4}	35
DNCO	(17 1 16 16–16 1 15 15)	348 599.7	174.6	6.10×10^{-4}	33
$HN^{13}CO$	(15 2 13 16–14 2 12 15)	329 594.5	299.2	5.08×10^{-4}	33
$HN^{13}CO$	(15 2 13 14–14 2 12 13)	329 594.5	299.2	5.06×10^{-4}	29
$HN^{13}CO$	(15 2 13 15–14 2 12 14)	329 594.5	299.2	5.06×10^{-4}	31
$HN^{13}CO$	(15 0 15 16–14 0 14 15)	329 673.4	126.6	5.18×10^{-4}	33
$HN^{13}CO$	(15 0 15 15–14 0 14 14)	329 673.4	126.6	5.16×10^{-4}	31
$HN^{13}CO$	(15 0 15 14–14 0 14 13)	329 673.4	126.6	5.15×10^{-4}	29
$HN^{13}CO$	(15 1 14 16–14 1 13 15)	330 860.2	170.2	5.21×10^{-4}	33
$HN^{13}CO$	(15 1 14 14–14 1 13 13)	330 860.2	170.2	5.19×10^{-4}	29
$HN^{13}CO$	(15 1 14 15–14 1 13 14)	330 860.2	170.2	5.19×10^{-4}	31
$HN^{13}CO$	(16 1 16 17–15 1 15 16)	350 340.3	186.1	6.20×10^{-4}	35
$HN^{13}CO$	(16 1 16 16–15 1 15 15)	350 340.3	186.1	6.18×10^{-4}	33
$HN^{13}CO$	(16 1 16 15–15 1 15 14)	350 340.3	186.1	6.18×10^{-4}	31
$HN^{13}CO$	(16 3 14 17–15 3 13 16)	351 427.6	531.9	6.07×10^{-4}	35
$HN^{13}CO$	(16 3 14 15–15 3 13 14)	351 427.6	531.9	6.04×10^{-4}	31
$HN^{13}CO$	(16 3 14 16–15 3 13 15)	351 427.7	531.9	6.04×10^{-4}	33
$HN^{13}CO$	(16 3 13 17–15 3 12 16)	351 427.7	531.9	6.07×10^{-4}	35
$HN^{13}CO$	(16 3 13 15–15 3 12 14)	351 427.7	531.9	6.04×10^{-4}	31
$HN^{13}CO$	(16 3 13 16–15 3 12 15)	351 427.7	531.9	6.04×10^{-4}	33
$HN^{13}CO$	(16 2 15 17–15 2 14 16)	351 548.3	316.1	6.19×10^{-4}	35
$HN^{13}CO$	(16 2 15 15–15 2 14 14)	351 548.3	316.1	6.17×10^{-4}	31
$HN^{13}CO$	(16 2 15 16–15 2 14 15)	351 548.3	316.1	6.17×10^{-4}	33
$HN^{13}CO$	(16 2 14 17–15 2 13 16)	351 561.8	316.1	6.19×10^{-4}	35
$HN^{13}CO$	(16 2 14 15–15 2 13 14)	351 561.8	316.1	6.17×10^{-4}	31
$HN^{13}CO$	(16 2 14 16–15 2 13 15)	351 561.8	316.1	6.17×10^{-4}	33
$HN^{13}CO$	(16 2 14 17–15 2 13 16)	351 561.8	316.1	6.19×10^{-4}	35
$HN^{13}CO$	(16 2 14 15–15 2 13 14)	351 561.8	316.1	6.17×10^{-4}	31
$HN^{13}CO$	(16 2 14 16–15 2 13 15)	351 561.8	316.1	6.17×10^{-4}	33
$HN^{13}CO$	(16 0 16 17–15 0 15 16)	351 642.9	143.5	6.30×10^{-4}	35
$HN^{13}CO$	(16 0 16 16–15 0 15 15)	351 642.9	143.5	6.27×10^{-4}	33
$HN^{13}CO$	(16 0 16 15–15 0 15 14)	351 642.9	143.5	6.27×10^{-4}	31

Appendix B: Additional figures

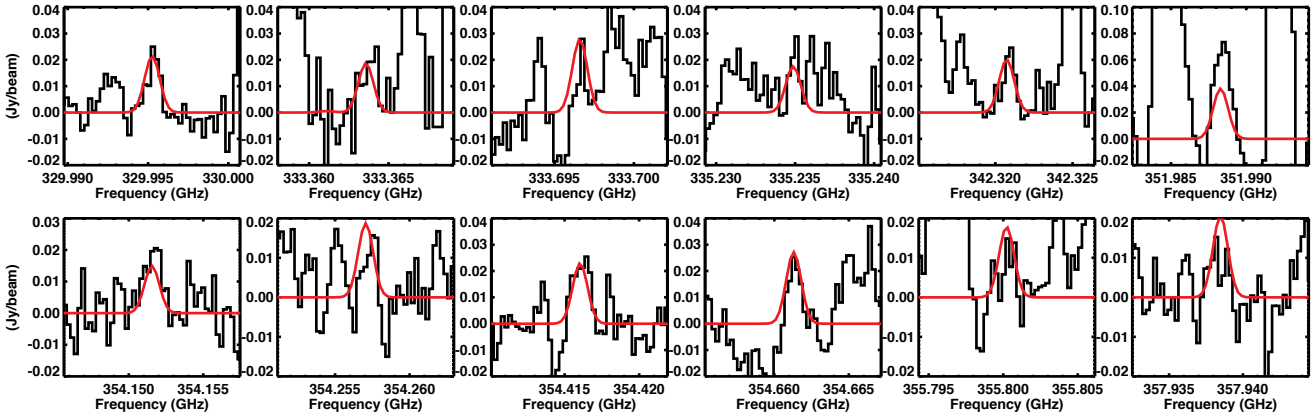

Fig. B.1. Black: detected lines of NH_2CDO. Red: best-fit model for T_{ex} = 300 K.

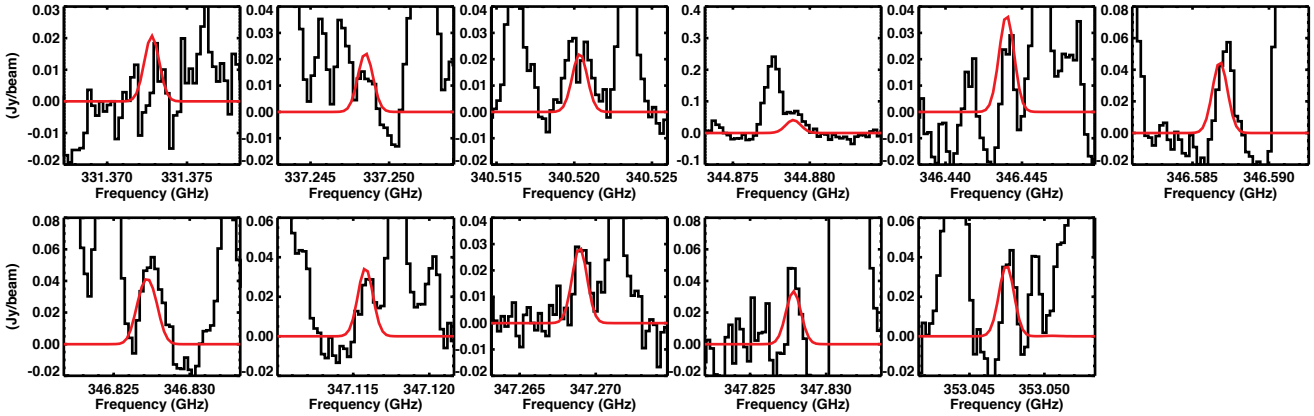

Fig. B.2. Black: detected lines of cis-NHDCHO. Red: best-fit model for T_{ex} = 300 K.

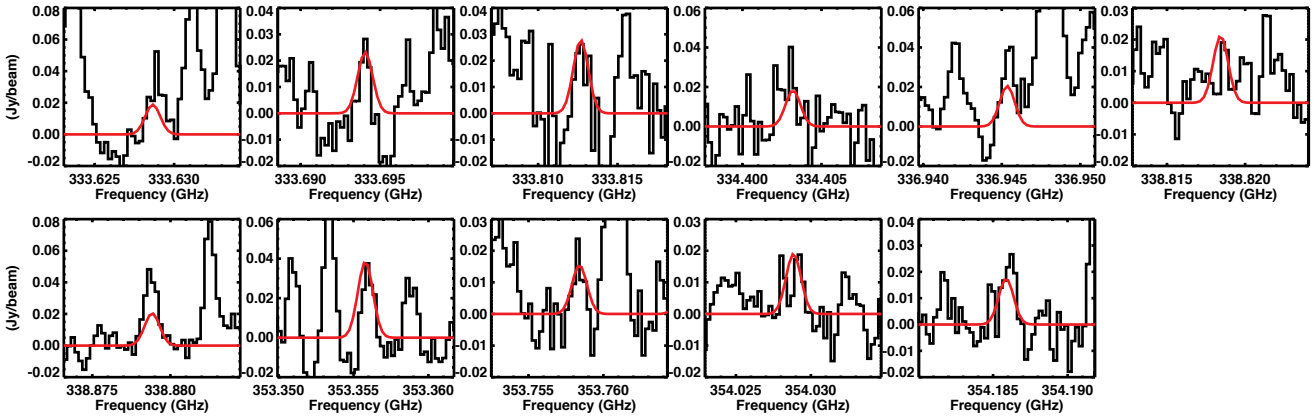

Fig. B.3. Black: detected lines of trans-NHDCHO. Red: best-fit model for T_{ex} = 300 K.

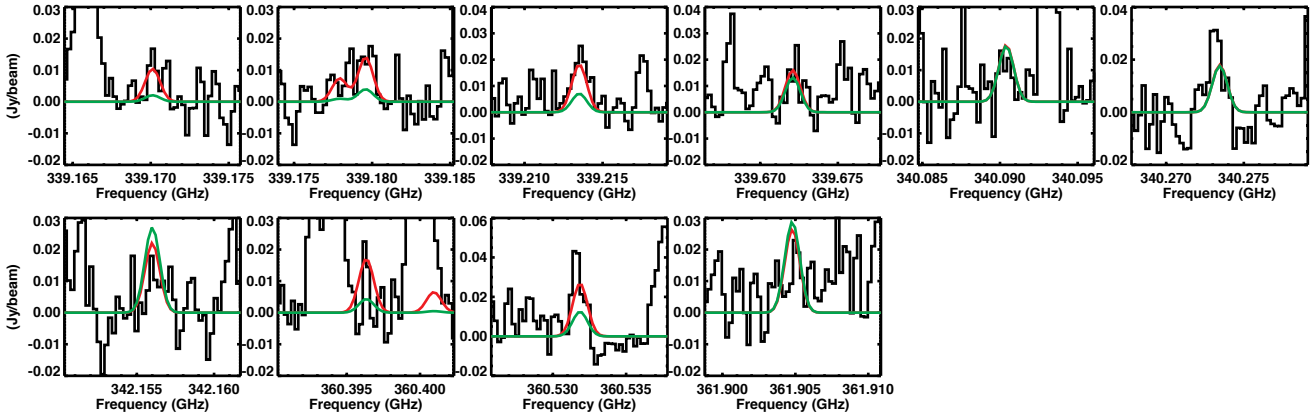

Fig. B.4. Black: detected lines of $NH_2^{13}CHO$. Red: best-fit model for T_{ex} = 300 K. Green: best-fit model for T_{ex} = 100 K.

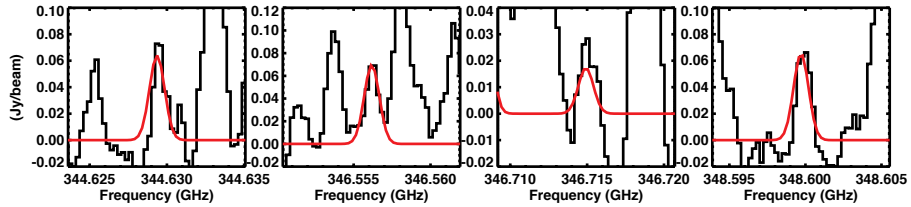

Fig. B.5. Black: detected lines of DNCO. Red: best-fit model for T_{ex} = 300 K.

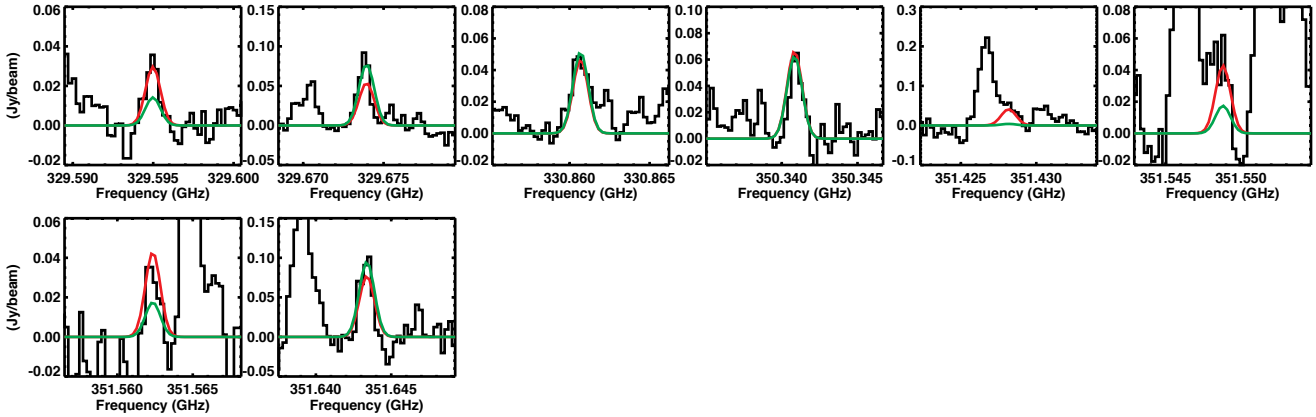

Fig. B.6. Black: detected lines of $HN^{13}CO$. Red: best-fit model for T_{ex} = 300 K. Green: best-fit model for T_{ex} = 100 K.

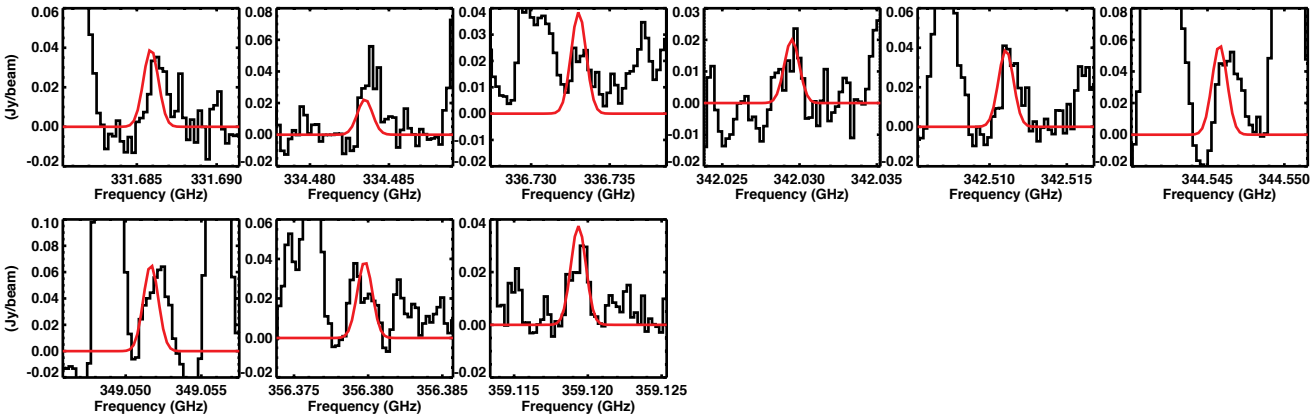

Fig. B.7. Black: lines of NH_2CHO v = 0 with the lowest opacities. Red: model based on the analysis of the $NH_2^{13}CHO$ lines and a $^{12}C/^{13}C$ ratio equal to 68.

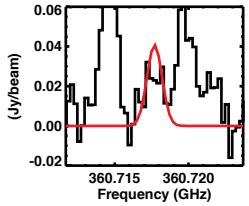

Fig. B.8. Black: line of NH_2CHO $v_{12} = 1$ with the lowest opacity. Red: model based on the analysis of the $NH_2^{13}CHO$ lines and a $^{12}C/^{13}C$ ratio equal to 68.